

# VARIATION OF PLASMA SPRAY DEPOSITS MICROSTRUCTURE AND PROPERTIES FORMED BY PARTICLES PASSING THROUGH DIFFERENT AREAS OF PLASMA JET

KAREL NEUFUSS, JAN ILAVSKÝ<sup>1,2</sup>, BLAHOŠLAV KOLMAN, JIŘÍ DUBSKÝ, PAVEL ROHAN, PAVEL CHRÁSKA

*Institute of Plasma Physics, Academy of Sciences CR,  
Za Slovankou 3, 182 21, Prague, Czech Republic  
E-mail: neufuss@ipp.cas.cz*

*Present affiliation:*

<sup>1</sup>*National Institute of Standards and Technology, Gaithersburg, MD, USA*

<sup>2</sup>*University of Maryland, College Park, MD, USA*

Submitted June 27, 2000; accepted November 8, 2000.

*Different trajectories of powder particles in the plasma jet during spraying result in different states of the particles/molten droplets on impact, resulting in the variation of microstructure and homogeneity of the deposits. The distribution of trajectories in the jet is related to the overall spray setup, i.e. to the spray parameters such as number and geometry of powder injectors, flow rate and type of the powder feeding gas, powder size distribution and its chemical and mechanical properties, etc. This paper studies the deposits microstructure and properties (density, porosity, phase composition, etc.) and relates them to the distribution of particles in the plasma jet during spraying. Free-standing tubes are selected then as an example of the industrially important application and their microstructure is compared with microstructures of flat samples documenting microstructure variation related to different particle trajectories in the jet. The two materials studied are Alumina ( $Al_2O_3 + 3wt.\% TiO_2$ ) and natural  $ZrSiO_4$ . Significant microstructure variation related to particle trajectories were found for alumina deposits; for example, the alpha phase content varied between about 5 and 50 %, the porosity volume varied between about 3.8 and 8 % (about 2x), and the pore surface area varied between about  $1.5 \times 10^4$  to about  $6.5 \times 10^4 \text{ cm}^2 \text{ cm}^{-3}$  (about 4x). Also the microstructure anisotropy documented by small-angle neutron scattering varied significantly. Variation in the microstructure of the  $ZrSiO_4$  seemed to be less significant.*

## INTRODUCTION

The trajectory of the particles through the plasma (or more generally thermal) jet, together with their morphology, size and chemistry determines their condition on impact. Particles traveling through the center of the jet are exposed to the fastest and hottest environment and have usually the highest velocities and temperatures. On the other hand, particles traveling through the outside layers of the jet exhibit usually lower temperatures and velocities [1]. This is reflected in their spreading behavior and, in larger picture, in the deposit microstructure and properties.

Since a single pass during thermal spraying rarely results in the deposit of sufficient thickness, most deposits are manufactured by spraying thin layers on top of each other by passing the torch over the substrate in "spray pattern". This procedure results in a sandwich like structure with observable layer boundaries [2]. Each layer is formed by subsequent deposition of particles traveling through different parts of the jet which overlap in a complex fashion. Therefore the layer itself exhibits through thickness variation of microstructure [3].

The substrate geometry can also significantly influence the deposit microstructure. As it was shown in

theoretical and experimental studies, impact angle of particles on the substrate can play a significant role in microstructure formation [4, 5, 6, 7]. It is important to note, that different materials have different level of sensitivity to this parameter. Major microstructure variations were found for Alumina ceramics, whereas some other ceramics (YSZ) and some metals exhibited much lower sensitivity [8].

Tubular substrates, rotating in a lathe, represent examples of relatively simple and common spray geometry for industrial applications such as wear and corrosion resistant pipes in chemical industry. However, even these "simple" substrates represent challenge since the overall spraying geometry is actually quite complex. Depending on the ratio of substrate size and size of the plasma jet, particles traveling through different parts of the jet are deposited at varying impact angles (figure 1). Therefore the resulting tube microstructure and properties cannot be simply related to the flat test coupons, as it is often done in practice. It is therefore necessary to spray number of test tubes when the spray process is optimized. This can be costly and can take extended time periods.

In this paper, variations of the microstructure in free standing ceramic tubes with varying diameters have

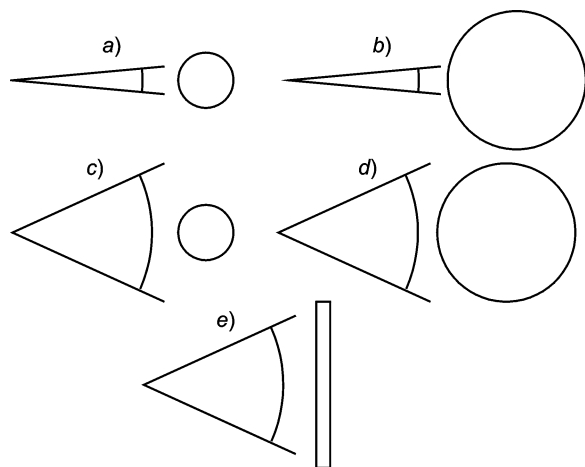


Figure 1. Four possible extreme scenarios of size relationships between the spray jet and tubular substrate size: a) small jet and small diameter substrate; b) small jet and large tube diameter; c) large jet and small tube diameter; d) large jet and large tube diameter; e) spraying flat test coupon.

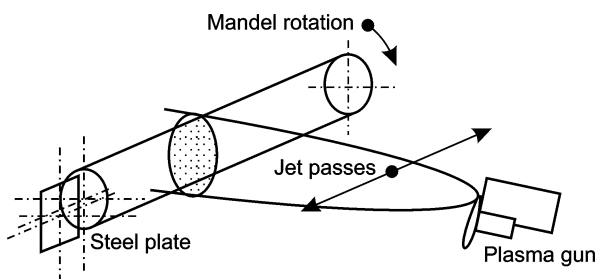


Figure 2. Spraying setup.

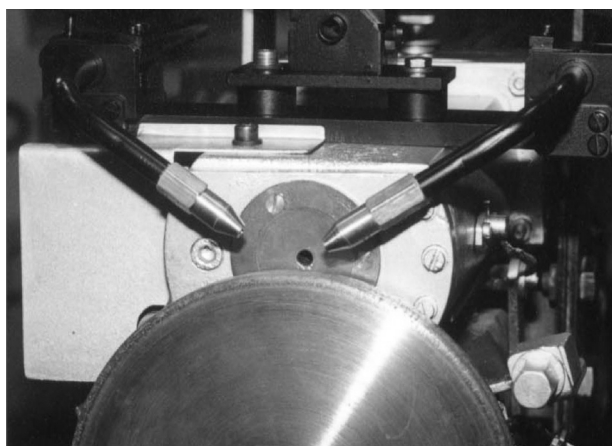


Figure 3. Front view - orientations of the powder feeders.

been studied and related then to the variations of microstructure and properties produced by particles passing through different areas of plasma jet and observed on a flat test sample.

## EXPERIMENTAL PART

Free-standing tubes were manufactured by spraying the ceramic powders on tubular iron mandrel preheated to various temperatures. The mandrels were horizontally mounted in a lathe and rotated with 60 rpm or 120 rpm. The lower rotational velocity was used for the larger diameter (96 mm) mandrel, the higher for mandrels with diameters 16, 54, and 79 mm. The spray process setup was selected so the mandrel temperature during spraying did not vary out of a preselected range. The spray system axis was aimed onto the rotational axis of the lathe (figure 2).

A steel plate of dimensions  $100 \times 80 \times 8$  mm (figure 2) was stationary mounted at the end of the lathe during spraying. The plate, at the same spraying distance as the mandrel, was preheated to the same temperature as the tubular mandrels prior to spraying and its temperature during spraying also did not vary out of the specified temperature range.

The spray system was passing horizontally over the length of the tubular mandrels as well as over the stationary plate during spraying. This resulted in formation of deposits with a uniform thickness on the mandrel and a spray pattern profile on the stationary plate. This profile was then used to study the variation of the microstructure and properties formed by particles traveling through different areas of plasma jet. Both, the tube and the spray pattern profile were stripped-off from the substrate on cooling due to a mismatch of the thermal expansion, as planned.

Two ceramic materials were studied – gray aluminum oxide ( $\text{Al}_2\text{O}_3$ , 3 wt.%  $\text{TiO}_2$ , 1 wt.%  $\text{Fe}_2\text{O}_3$ ), henceforward “Alumina”, and zirconium silicate ( $\text{ZrSiO}_4$ ) = “Zircon”. The Alumina was supplied by Carborundum Electrite a.s. Benátky nad Jizerou, under name: “korund 96 A Ib č. 230”; Zircon is natural Australian sand, ground and cut to needed size distribution. The used powder sizes of these materials were: 40 - 63  $\mu\text{m}$  for Alumina and 40 - 70  $\mu\text{m}$  for Zircon. The water stabilized plasma spray system WSP<sup>®</sup> 500 (IPP AS CR Prague, Czech Rep.) was used. This spray system offers high spray throughput together with flexibility in the spray setup. Two external powder feeders were used (figure 3). The feeding gas was air, feed rates were about  $25 \pm 1$   $\text{kg h}^{-1}$  for Alumina and  $27 \pm 1$   $\text{kg h}^{-1}$  for Zircon. Feeding distances (distance between the torch nozzle and the injectors) were optimized for each material separately to ensure maximum degree of melting and were 30 mm for Alumina and 25 mm for Zircon. The injectors were pointing downstream to the spray axis at an angle about  $75^\circ$ . The spray distance (distance between the torch nozzle and substrate) were 350 mm for both materials.

## MEASUREMENT PROCEDURES

Samples were cut from the free-standing tubes and the spray pattern profile using a diamond saw. Samples from the spray pattern profile (figure 4) were cut in 10

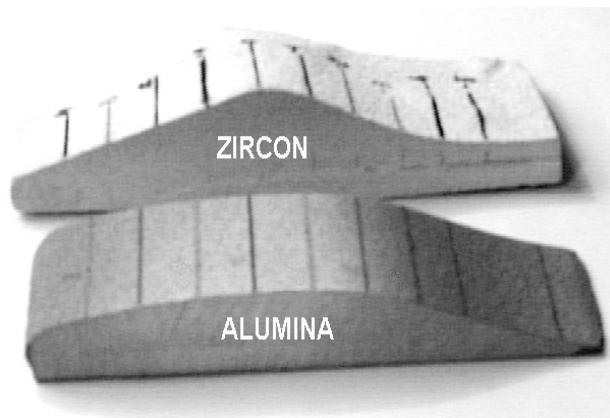


Figure 4. Spray pattern profiles formed on the flat steel substrate.

different vertical distances from the axis of the lathe (1 cm apart). This allowed studying the properties and microstructure formed by particles passing through different areas of the jet.

Porosity was measured by Archimedeian (water immersion) method, described elsewhere [9]. This method allows to measure density to about  $\pm 0.002 \text{ g cm}^{-3}$  and open porosity to about  $\pm 0.1\%$ . Density of the samples was also measured by Helium pycnometry (Micro-meritics, USA) with precision about  $\pm 0.0016 \text{ g cm}^{-3}$ .

Phase composition of Alumina samples, i.e. the content of alpha = "corundum"- phase was determined by two methods - by XRD measurement [10] and by density measurement. In the later case, the density was calculated using the following relation:  $\gamma_m = 3.99 \cdot x + (1-x) \cdot 3.647$  (where  $x$  is content of  $\alpha\text{-Al}_2\text{O}_3$  and  $\gamma_m$  is the measured density). Densities of  $\gamma\text{-Al}_2\text{O}_3 = 3.647 \text{ g cm}^{-3}$  and  $\alpha\text{-Al}_2\text{O}_3 = 3.99 \text{ g cm}^{-3}$  were assumed [11].

Microstructure of the Alumina spray pattern profile sample was also studied using anisotropic Porod method of the small-angle neutron scattering (SANS). This method, described elsewhere [4], allows quantitative surface characterization of the voids within the microstructure by their specific surface area and by anisotropy of the scattering. In samples with a strong anisotropy it is often possible to characterize separately the two dominating void systems – interlamellar voids and intralamellar cracks. As it was already documented, phase transformations in Alumina deposits result in significant increase of the cracks specific surface area and in overall reduction of microstructure anisotropy [12, 13].

## RESULTS AND DISCUSSION

Figure 1 shows, that when tubular substrates are used, there are basically three possible scenarios when size of spray pattern and substrate diameter are compared. The spray pattern can be significantly larger (figure 1c), comparable (figures 1a and 1d) or smaller

(figure 1b). Only in the case 1b) the approximation by a flat experimental test coupon (figure 1e) is acceptable. In all other cases large differences in microstructures between the tubes and flat test samples can be expected. Cases when the spray pattern is smaller or comparable (figures 1a, b, and d) to the substrate size are the best from the point of view of deposition efficiency. Spraying tube with diameter of 16 mm with the WSP® spray system results in low deposition efficiency, since most of the sprayed particles miss the substrate.

Significant differences between cases in figures 1b and c are in variations of impact angles (given by the substrate shape) and of particle impact conditions (given by the distribution of particles within the spray pattern). Therefore in the case in figure 1b one can expect minimum variation of the impact angle, whereas for 1c one can expect minimum variation of particle impact properties. In this case, due to size of the substrate, particles passing through the center of the jet are deposited.

Since the distribution of particle properties within the spray pattern profile may be significant, if the aim of the spraying is to produce the most homogeneous microstructure at any cost, it may be necessary to select small substrate diameter and accept large amount of overspray (and possibly to utilize some feedstock recycling methods). This method may be especially successful for materials whose deposit properties are not too sensitive to impact angles, such as Zirconia (YSZ) ceramics [8].

Figure 5 shows, that for both materials the spray profile is asymmetric. While this should be clearly related to the plasma jet properties variations, to geometry of feeding systems and the to feeding setup in general, it is also related to the feedstock material, to its particle size distribution, density, shape and geometry. In the present case the differences in physical properties of the feedstock materials (table 1) cause consequently significant differences in the distribution of particles in the jet.

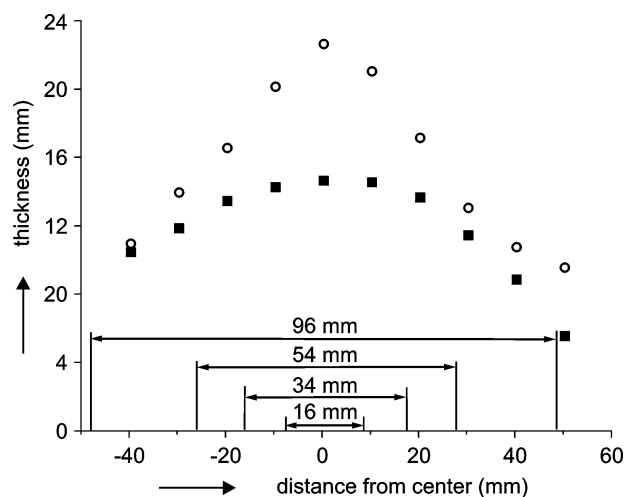


Figure 5. Thickness profiles for both sprayed materials. ■ - Aluminas, ○ - Zircon

Table 1. Data for feedstock powders.

feedstock powder material	density (g cm <sup>-3</sup> )	heat of melting (kJ kg <sup>-1</sup> )
Alumina	3.99	2659
Zircon	4.62	1400 - 1796

The phase composition of feedstock materials was alpha phase for Alumina and Zircon phase for ZrSiO<sub>4</sub>. Due to rapid solidification the phase composition changed for the deposits and is discussed lower.

In order to ensure formation of deposits with acceptable microstructure it was necessary to have different feeding distance. Even though Zircon requires lower heat for melting, it needed to be fed into warmer parts of plasma jet (25 mm from the nozzle) than Alumina (30 mm from the nozzle) in order to be melted. This is most likely related to the different thermal conductivity of these materials and to the well known dissociation of ZrSiO<sub>4</sub> into ZrO<sub>2</sub> and SiO<sub>2</sub> on spraying. Both - different feeding distance and different density - are probably responsible for the differences in the spray pattern (figure 4).

#### Alumina

Table 2 and figure 6 summarize the measured data for Alumina. Comparison of figure 5 and figure 6 shows, that apparent density and the profile thickness have maxima at the same place. Open porosity increases towards the edges of the spray pattern profile, which is probably related to the decrease of the average velocities and temperatures of the particles passing through the jet edges. However, the central parts of the

spray pattern profile also exhibit higher porosity. This is most likely related to formation of larger amount of alpha Alumina phase in this region, caused by local overheating in this area during successive passes. The measured substrate temperature in the center of the spray pattern for the used spraying parameters was higher than for normally used parameters, reaching as high as 480 °C, while 30 mm from the center the maximum temperature was only about 380 °C. While usually the thermally sprayed alumina deposits are composed mostly from gamma (metastable) phase, local high temperatures can cause gamma phase of Alumina to transform into alpha phase. Since these phases have significantly different densities (3.647 g cm<sup>-3</sup> and 3.99 g cm<sup>-3</sup>) this transformation results in an increase of porosity.

Higher porosity (cracks - see discussion later) has been observed in the center of the Alumina sample which corresponds to a significant increase of alpha phase content in this region. Both methods for measurements of the alpha phase content give similar results - maximum in the center of the spray pattern profile (40 - 50 % of alpha phase) and minimum in tails (1 to 5 %). The differences may be caused by different measured volume - XRD measures only surface layers of the sample, whereas the density method measures the whole volume and thus any local variations in the phase content are likely to influence the density method much less. On the other hand, presence of closed porosity can limit precision of the density method.

The change in microstructure related to phase transformation was confirmed by SANS results (figure 7). Significant increase of the crack specific surface area is probably related to the fine cracks formed during gamma to alpha Al<sub>2</sub>O<sub>3</sub> phase transformation. If the alpha phase were present from the spraying, there would be no material density change and these fine voids would not be formed.

Table 2. Summary of data for all Alumina samples.

sample	distance from the torch axis or tube diameter (mm)	deposit thickness (mm)	apparent density $\gamma^o$ (g cm <sup>-3</sup> )	open porosity (%)	residual density (g cm <sup>-3</sup> )	fraction of $\alpha$ phase XRD (%)	fraction of $\alpha$ phase from density (%)
ATR1	40	10.5	3.372	5.5	3.6827	9.8	10.4
ATR2	30	11.9	3.454	3.8	3.6796	9.1	9.5
ATR3	20	13.5	3.480	3.8	3.6859	11.5	11.3
ATR4	10	14.3	3.517	4.5	3.7418	31.7	27.6
ATR5	0	14.7	3.536	4.9	3.7747	47.8	37.2
ATR6	10	14.6	3.533	4.7	3.7560	42.0	31.2
ATR7	20	13.7	3.505	3.8	3.6998	16.2	15.4
ATR8	30	11.5	3.478	3.7	3.6517	5.1	1.4
ATR9	40	8.9	3.441	3.9	3.6493	9.5	0.8
ATR10	50	5.6	3.282	8.0	3.6648	16.6	5.2
ATUBE16	diameter 16	1.8	3.300	7.3	3.6738	17.7	7.8
ATUBE34	diameter 34	3.5	3.440	3.8	3.6635	6.7	4.8
ATUBE54	diameter 54	2.3	3.360	5.3	3.6545	13.9	2.2
ATUBE96	diameter 96	4.4	3.340	5.2	3.6700	4.7	6.7

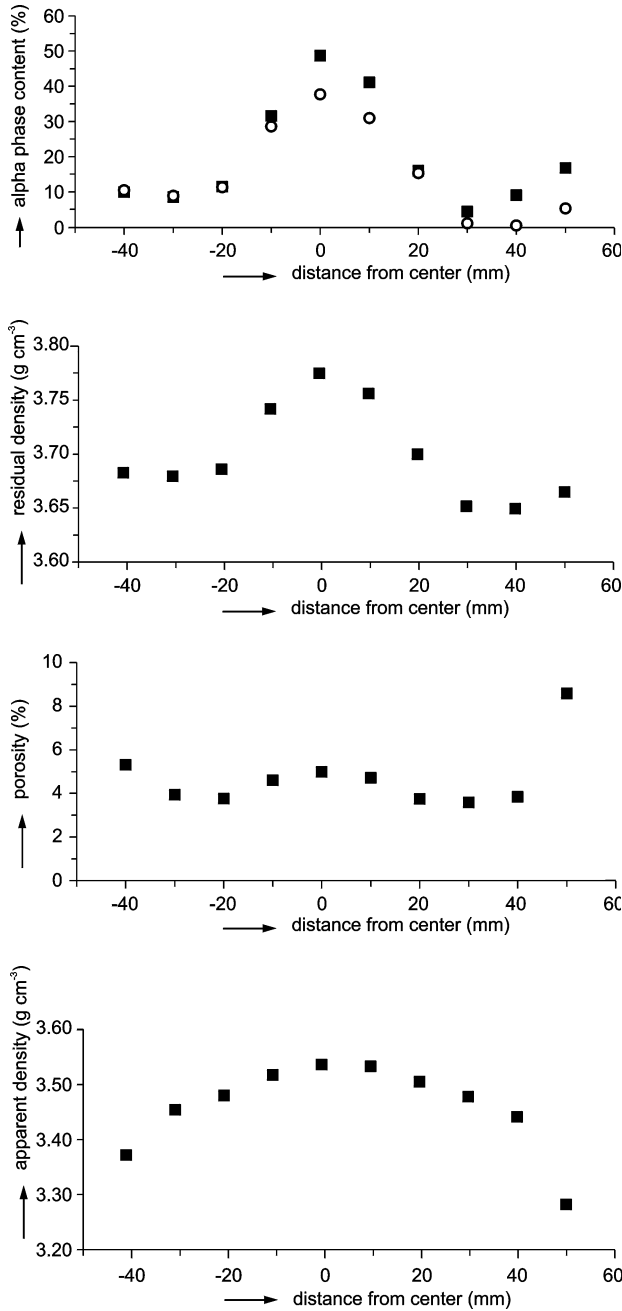


Figure 6. Results for Alumina spray pattern.  
 ■ - XRD measured, ○ - density calculated

The change in anisotropy can be observed in figure 8 and figure 9. Detailed explanation of these graphs can be found in [4]. For the current presentation it is sufficient to note, that these figures represent anisotropy of values of the Porod constants evaluated in different directions in the sample.

Vertical spheroid represents surfaces of voids with preferred orientation parallel with the substrate while horizontal spheroid represents surfaces of voids mostly perpendicular to the substrate. Figure 8 exhibits nearly

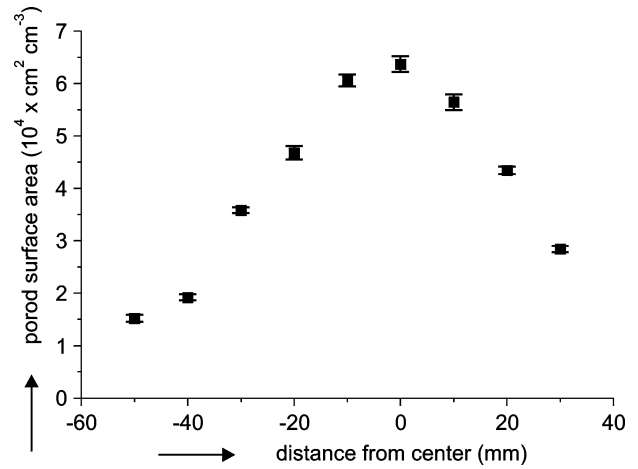


Figure 7. Results of SANS surface area characterization of Alumina spray pattern profile.

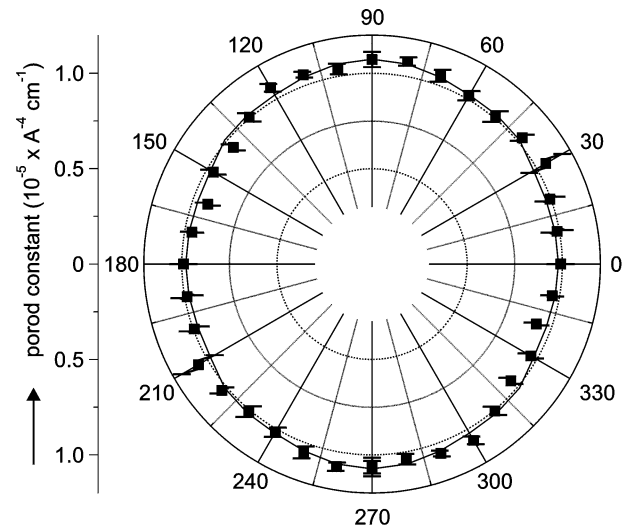


Figure 8. Anisotropic Porod scattering for sample from the center of the Alumina spray pattern.

spherical shape and high values of Porod constant, which confirms that the void system in this sample is nearly isotropic with a high surface area. Figure 9 shows much lower values of Porod constants and clearly observable anisotropy. Note, that as it was shown in [14], this anisotropic shape is composed of two nearly ellipsoid-like shapes representing two major void systems in these materials - interlamellar pores and interlamellar cracks. Interlamellar cracks can be created either during cooling of the splats, when these relax cooling stresses, or during phase transformation of Alumina due to density difference between the gamma and alpha phase. While the transformation cracks have isotropic orientation distribution, cooling cracks have preferred orientation perpendicular to the substrate.

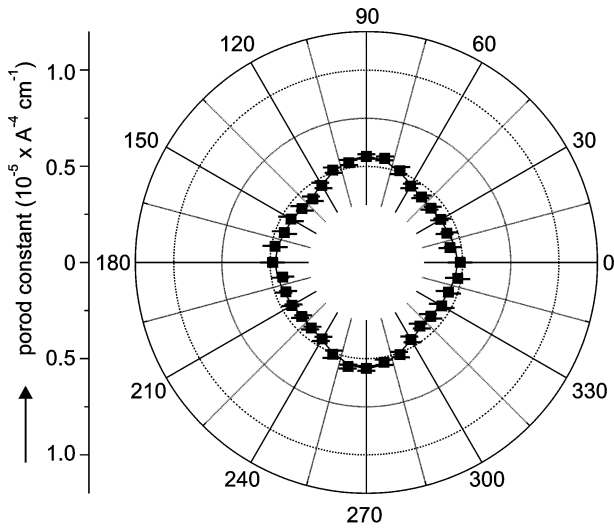


Figure 9. Anisotropic Porod scattering from sample 3 cm from the center of Alumina spray pattern.

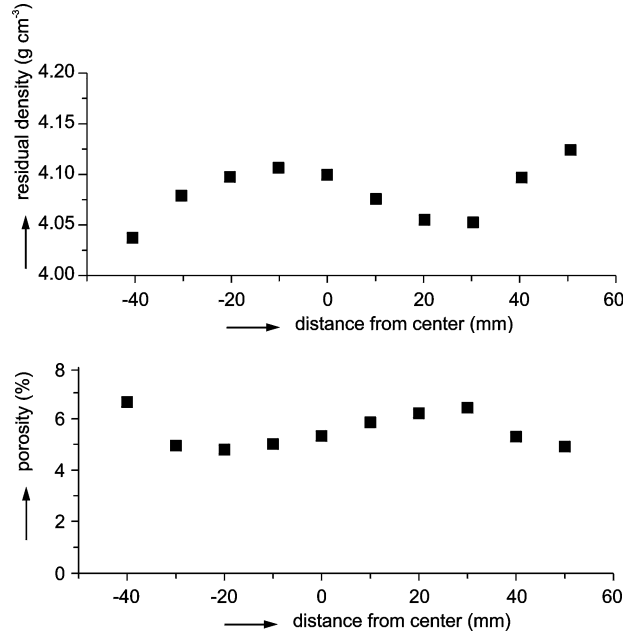


Figure 10. Open porosity for the Alumina free standing tubes.

It is interesting to note that the plasma sprayed tubes exhibit dependency of porosity on their diameter (figure 10). This is likely related to the geometry, when for the small diameter tube the spray geometry resembles mostly case *c*) from figure 1, while the other tube diameters are getting closer to case *d*). The reason for a minimum at 34 mm is probably the fact, that with this diameter mainly the central part of the sprayed particles - the particles well molten and with the highest impact speeds - is deposited because of the substrate size. This is, of course, true only in direction perpendicular to the axis of the tube. Probably a much lower porosity could be obtained when all the particles outside of some pre-selected distance from the center of the plume in horizontal direction could reasonably well mask off.

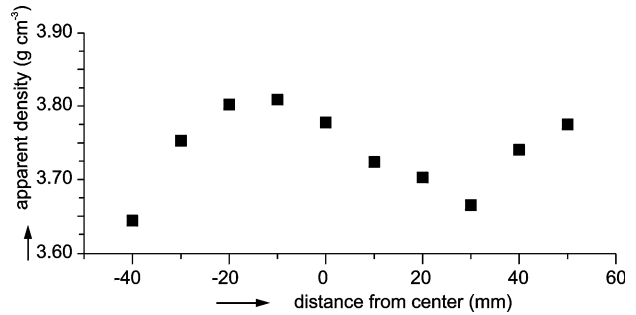


Figure 11. Results for Zircon spray pattern.

Further reason for increase of porosity at higher diameter tubes is the difference in the peripheral speeds. For 54 mm diameter tube this speed reaches over  $350 \text{ mm s}^{-1}$  while it is around  $300 \text{ mm s}^{-1}$  for the 96 mm tube, where the rotational speed was lowered to 60 rpm.

#### Zircon

This material exhibits more symmetric spray pattern profile (figures 4 and 5) compared with that for Alumina. Likely reason for it may be that the feeding distance was shorter and thus the trajectories of injected particles in the plasma jet were different. In general, the density of this material is higher and exhibits also more complex profile of the density and porosity (figure 11), however, overall variations are significantly lower than for Alumina. This profile exhibits in one direction from the center decrease in porosity and increase in densities. This is most likely related to the asymmetric feeding system. The feeding system on the used torch consists of two individual feeders from top (figure 3). Therefore, denser and larger particles may travel through the plasma and in some distance from the center may be

Table 3. Summary of results for all Zircon samples.

sample	distance from the torch axis or tube diameter (mm)	deposit thickness (mm)	apparent density $\gamma^0$ (g cm <sup>-3</sup> )	open porosity (%)	residual density (g cm <sup>-3</sup> )
ZTR1	-40	11.0	3.642	6.6	4.035
ZTR2	-30	14.0	3.761	5.0	4.076
ZTR3	-20	16.6	3.799	4.8	4.095
ZTR4	-10	20.2	3.806	5.0	4.104
ZTR5	0	22.7	3.785	5.3	4.096
ZTR6	10	21.1	3.748	5.9	4.072
ZTR7	20	17.2	3.704	6.2	4.052
ZTR8	30	13.1	3.666	6.4	4.050
ZTR9	40	10.8	3.714	5.3	4.095
ZTR10	50	9.6	3.772	4.9	4.120
ZTUBE16	diameter 16	2.1	3.740	5.7	4.109
ZTUBE34	diameter 34	1.8	3.758	5.4	na
ZTUBE54	diameter 54	2.4	3.691	6.2	4.028

more of particles of certain size and density. Interestingly, there seems to be little effect of this phenomenon on the thickness of the deposit. Tubes sprayed from this material show smaller variations in porosity and densities (table 3). However, more experimental work is needed to explain these results. Very well known decomposition of Zircon on spraying into crystalline Zirconia and glassy Silica leaves an open question about the role of Silica which could, partly compensate, for instance, the effects of the spraying set up.

### CONCLUSIONS

The two ceramic materials used in this study exhibit significantly different behavior. Zircon seems to be more forgiving with respect to spraying tubes of different diameters and resulting variations in their microstructure. This may be due to decomposition of Zircon on spraying, when other important changes may, to some extent, suppress the influence of spraying parameters. Alumina is more sensitive and shows complex changes caused by phenomena like impact angle, local overheating and resulting phase transformations and selection of particles traveling through different areas of plasma plume.

### Acknowledgment

This work has been partially supported by grants of the Grant Agency of the Czech Republic no. 106/97/S008 and 104/99/0304.

### References

1. Herman H.: Scientific American 259, 112 (1988).
2. Ohmori A, Li C.: Thin Solid Films 201, 241 (1991).

3. Wallace J., Ilavský J.: J. Thermal Spray Technology 7, 521 (1998).
4. Ilavský J., Allen A. J., Long G.G., Krueger S., Berndt C.C., Herman H.: J.Am.Ceram. Soc. 80, 733 (1997).
5. Leigh S.H., Berndt C.C.: Surf Coat Tech. 89, 213 (1997).
6. Montavon G., Sampath S., Berndt C. C., Herman H., Coddet C.: Surf Coat Tech 91, 107 (1997).
7. Hennaut J., Othmezzouri J., Charlier J.: Mater Sci Technol 11, 174 (1995).
8. Ilavský J., Kolman J., Neufuss K., Chráska P.: Proc. of the 2<sup>nd</sup> United Thermal Spray Conference UTSC '99, p.820, Editors: E. Lugscheider and P. A. Kammer, DVS Verlag, Düsseldorf, 1999.
9. Neufuss K., Chráska P., Kolman B., Sampath S., Trávníček Z.: J. Thermal Spray Technology 6, 434 (1997).
10. Ilavský J., Berndt C.C., Herman H., Chráska P., Dubský J.: J. Thermal Spray Technology 6, 439 (1997).
11. Ilavský J.: p.203, in *Materials Science and Engineering*, State University of New York: Stony Brook, 1994.
12. Ilavský J., Herman H., Berndt C.C., Goland A.N., Long G.G., Krueger S., Allen, A.J.: Proceedings of the 6<sup>th</sup> National Thermal Spray Conference - *Thermal Spray Industrial Applications*, Boston USA, p.709, Eds.: C.C. Berndt, S. Sampath, ASM International, Materials Park, Ohio, USA 1994.
13. Ilavský J., Allen A.J., Long G.G., Krueger S., Herman H., Berndt C.C., Goland, A.N.: Proceedings of the 14<sup>th</sup> International Thermal Spray Conference: *Thermal Spraying-Current Status and Future Trends*, Kobe, Japan, p. 483, Edited by A. Ohmori, High Temperature Society of Japan, 1995.
14. Ilavský J., Long G.G., Allen A.J., Herman H., Berndt C.C.: Ceramic-Silikáty 42, 81 (1998).

Submitted in English by the authors.

PROFIL STOPY PLAZMOVÉHO NANÁŠENÍ  
A VLASTNOSTI NANESENÝCH VRSTEV

KAREL NEUFUSS, JAN ILAVSKÝ<sup>1,2</sup>,  
BLAHOŠLAV KOLMAN,  
JIŘÍ DUBSKÝ, PAVEL ROHAN, PAVEL CHRÁSKA

Ústav fyziky plazmatu, AVČR,  
Za Slovankou 3, 182 21, Praha

Současná adresa:

<sup>1</sup> National Institute of Standards and Technology,  
Gaithersburg, MD, USA,

<sup>2</sup> University of Maryland, College Park, MD, USA

Rozložení částic v proudu plazmatu během plazmového nanášení má zásadní význam při vytváření povlaků. Toto rozložení však není stabilní (konstantní), mění se vlivem fluktuací plazmatu, turbulencí přisávaného vzduchu a dále vlivem řady technologických parametrů (geometrie a počet vnášecích přívodů, granulometrie, hustota a vlastnosti

nanášeného materiálu a parametry plazmatu). Vytvořené povlaky jsou tedy důsledkem nestabilních a stabilních procesů, které jsou dále "průměrovány" technologickým postupem (počet nanášecích cyklů a rozměry upravovaného předmětu).

Na rozložení částic v proudu plazmatu je možné usuzovat z profilu nanášecí stopy, případně ze změn kvality vytvořených povlaků (struktura, pórovitost, fázové složení, CTE). Článek je proto věnován vybraným vlastnostem jednotlivých částí profilu stop dvou různých materiálů: syntetického  $Al_2O_3+3$  hmotn.%  $TiO_2$  a přírodního zirkonu  $ZrSiO_4$ . Profily stop byly vytvořeny jako "vedlejší" produkt při výrobě samonosných keramických trubek různého průměru. Vybrané vlastnosti naměřené na profilu stopy jsou v článku porovnávány s vlastnostmi vrstev získaných ze samonosných trubek.

Pro plazmové nanášení bylo použito hořáku s vodní stabilizací elektrického oblouku WSP 500<sup>®</sup> (s vyšší entalpií než klasické plazmové hořáky) a pro studium vlastností povlaků a vrstev byly použity vedle klasických metod i některé méně obvyklé metody jako např. malouhlový neutronový rozptyl.